

Damage Analysis of Composite CFRP Tubes Using Acoustic Emission Monitoring

ŠOFER M.^{1,a}, CIENCIALA J.^{1,b}, FUSEK M.^{1,c}, PAVLÍČEK P.^{1,d},
MORAVEC R.^{2,e}

¹Department of Applied Mechanics, Faculty of Mechanical Engineering, VŠB – Technical University of Ostrava, 17. listopadu 2172/15, 708 00 Ostrava, Czech Republic

² Havel Composites CZ s.r.o., Svěsedlice 67, 783 54 Přáslavice, Czech Republic

^amichal.sofer@vsb.cz, ^bjakub.cienciala@vsb.cz, ^cmartin.fusek@vsb.cz,
^dpavel.pavlicek@vsb.cz, ^emoravec@havel-composites.com

Keywords: Acoustic emission; CFRP composites; Unsupervised learning; Paddle

Abstract. The utilization of acoustic emission monitoring across different sectors with various applications is evident especially in the field of composites. In this work, three carbon fiber reinforced polymer composite tube types, intended for paddle production, are subjected to mechanical bending test up to their ultimate limit. With the use of acoustic emission monitoring and subsequent postprocessing of the data by unsupervised pattern recognition approach, it was possible to characterize the damage evolution for given composite tube type.

Introduction

Over the past decades, carbon fiber reinforced polymer (CFRP) composites have shown a constant increase in a variety of applications such as car or aircraft components, sports and medical equipment [1] and recently also in additive manufacturing [2-4]. Their main benefit lies primarily in relatively large strength/weight ratio or the ability to customize the material properties for dedicated purposes by changing the stacking sequence and related fiber orientation. One of the specific sectors, where the CFRP composites are widely applied, is canoeing with related manufacturing of the paddles. This sport equipment is during its lifecycle exposed to cycling bending, which can, besides the material aging process, to a certain extent affect the paddle stiffness. The basic study of the mechanical response of given structure, in our case the CFRP composite tube forming the paddle, can be realized using universal testing machine with dedicated equipment. To gain more detailed insight into damage monitoring process on micro-scale, we have to incorporate any additional method such as acoustic emission (AE) testing [5]. AE monitoring during mechanical loading of given structure is an effective tool for studying the evolution of damage processes in the material [6]. Generally, the method is even capable of detecting the onset of plastic deformation [7], which has the character of white noise with low energy [8]. The advantages of the AE method are apparent in the case of analysis of more complex materials such as composites. The main objective of the presented study is to experimentally simulate the operation of the three types of CFRP paddle tubes to its ultimate limit state including monitoring the damage evolution process using AE method. The measured AE data are subsequently analyzed with use of unsupervised pattern recognition approach. Based on the reported signal properties of different failure modes in composites from various studies, the authors were able to classify the measured AE signals accordingly.

Test sample characterization

The experiments were carried out on three types of CFRP tubes with different number of layers, their orientation and woven fiber density of used material (see Figure 1), where each type of CFRP tube has been represented by three test samples. Samples labeled as „A“ were manufactured using four layers of unidirectional carbon woven fabric with density 200 g/m^2 and one layer of aramid/carbon woven fabric $[0^\circ\text{-}90^\circ]$ with density 175 g/m^2 and average wall thickness of 1,45 mm. The production of samples labeled as „B“ included the use of two layers of unidirectional carbon woven fabric with density 300 g/m^2 and one layer of carbon woven fabric $[0^\circ\text{-}90^\circ]$ with density 280 g/m^2 with average wall thickness of 0,9 mm, while samples labeled as „C“ were manufactured using solely four layers of unidirectional carbon woven fabric with density 300 g/m^2 with average wall thickness of 1,42 mm.

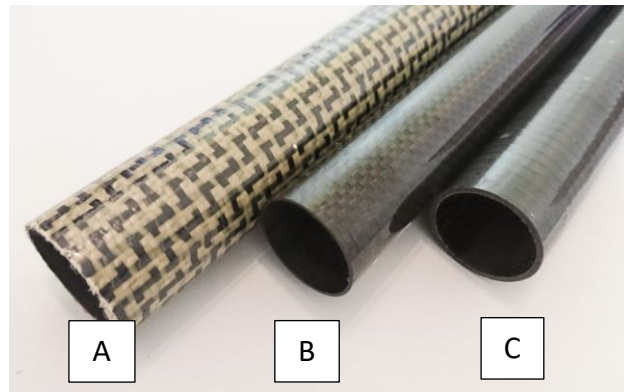


Fig. 1: CFRP composite tubes under test

Experimental procedure

Three point bending test procedure has been selected in order to simulate as much as possible the real nature of the loading process during the use of the paddle. The realization of the experiments was carried out on universal testing machine Testometric M500-50CT with dedicated weldment, which enables with its moving parts to modify its geometry for a wide variety of such experiments. The distance between the supports was equal to 1040 millimeters, while the force has been acting 440 millimeters from AE sensor #1 (see Fig. 2).

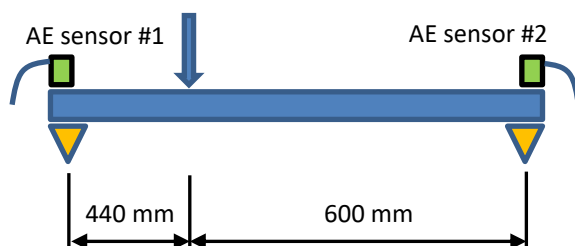
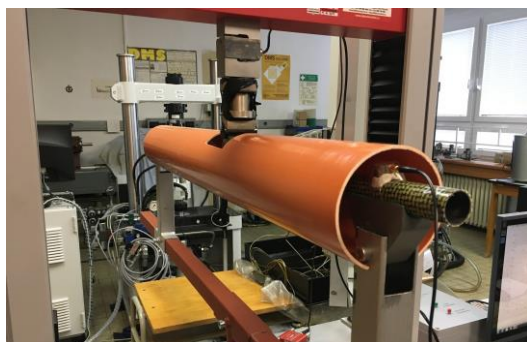


Fig. 2: In-Situ photograph of the test rig including specimen equipped with AE sensors (left); schematic representation of the three point bending test (right)

The tested tube with attached AE sensors was placed in a plastic pipe to prevent damage to the AE sensors and other equipment due to sudden integrity violation. The supports were covered by thin felt to allow free movement of the tube during its bending. The test has been deformation-controlled with the the upper anvil speed equal to 10 mm/min.

Acoustic emission monitoring

The acoustic emission activity was monitored using Vallen AMSY-6 AE system with two utilized measuring channels (ASIP-2A dual channel signal processor card), equipped with AEP5H 34 dB preamplifiers and broad-band Vallen VS-900 AE sensors, which have been attached onto the tube with use of oil-based plasticine. The sampling frequency of the AE data was set to 10 MHz while the transient data (wave transients) were sampled with 20 MHz and frequency range between 50 and 1100 kHz. Since the AE sources, which will occur in the close vicinity of the force acting point, will be located at a relatively greater distance and, at the same time, the composite exhibits higher rate of signal attenuation, it was necessary to set a lower value of threshold, in our case equal to 32 dB. The measured data were then filtered using the linear localization condition, for which has been known the approximate AE source location, i.e. force acting point at the distance of 440 mm from AE sensor #1 (see Fig. 2).

The filtered data were followingly analyzed with Vallen VisualClass software package, which uses the pattern recognition method [9] to associate similar waveform types into separate groups. Due to the nature of the task, an unsupervised learning approach [10] was chosen. The procedure starts with loading the selected database into Vallen VisualClass software, where in the beginning, the user has to specify the number of time windows including their span and the starting point in the time domain related to the origin defined by detection threshold (see Figure 3 - left).

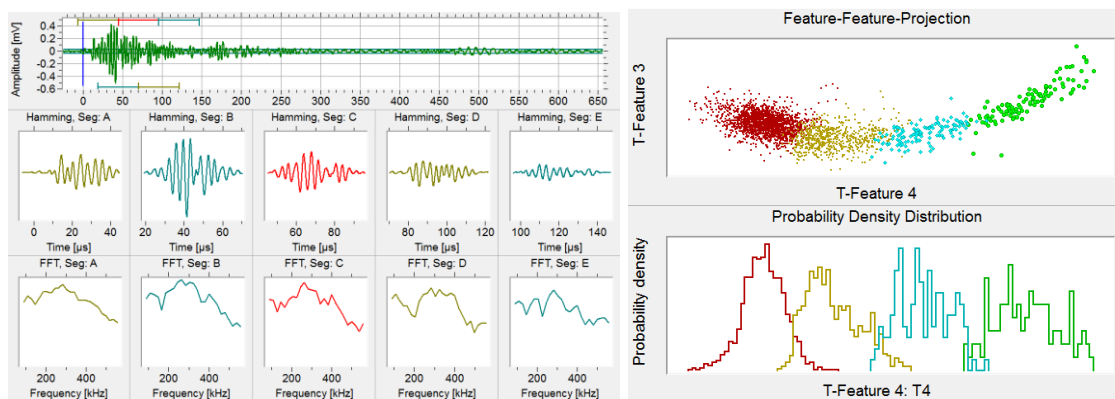


Fig. 3: Setting up the Hamming windowed time segments with corresponding results in frequency domain (left); Transformed features projection – results for four selected clusters (right)

The current analysis incorporates following settings: Number of time segments: 5; Size of single time segment in terms of points: 1024; Rel. trigger offset: -128 points; min/max frequency limit: 50/700 kHz. The software then performs the assembly of multidimensional feature vector, which size depends on the chosen number of time segments including their size. After the calculation process will be obtained the basic feature space, which is then linearly transformed for maximizing inter-class distance and minimizing the intra-class extension, at the same time (see Figure 3 - right). The results are then transferred into VisualAE software for further postprocessing. Four clusters were chosen for subsequent analysis, since the additional increase of the number of clusters did not lead to better differentiation of individual transients. One sample from each series has been subjected to the attenuation measurement of the AE signal in order to properly display the real AE signal amplitude in subsequent data analysis. The results of the attenuation measurement are shown in table 1.

Table 1: Attenuation measurement

Sample series	Near field attenuation [dB/m]	Far field attenuation [dB/m]
A	90	33,3
B	66,6	33,2
C	222,2	36,2

Results and discussion

Figure 4 shows relation between force and displacement of the anvil for individual A/B/C production run samples. The highest stiffness is being reached by C series samples, followed by A and B series samples. All three manufacturing modifications show within their group very similar trend in terms of the force-displacement course except A series sample A2, which exhibits marginally lower stiffness.

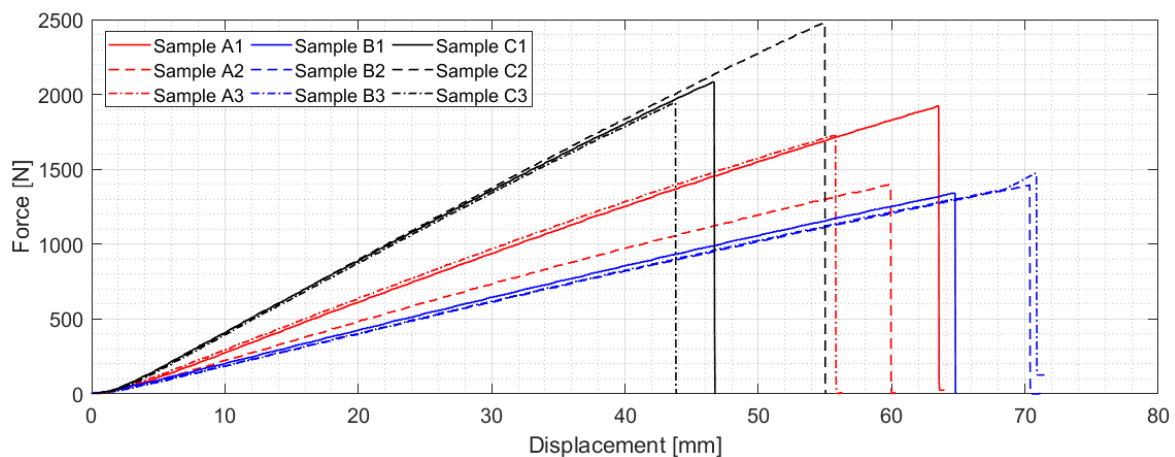


Fig. 4: Force as the function of displacement for individual A/B/C production run samples

The above conclusion however is not valid for the maximum force across individual series, where can be registered differences from 10 to 28 percent related to the maximal achieved force in each production run. The reason for the results variation can be found in the production itself. A somewhat similar trend can be registered in case of number of located AE events across the $0 \rightarrow F_{\max}$ range for individual samples (see Figure 5), where a relatively large variation is registered.

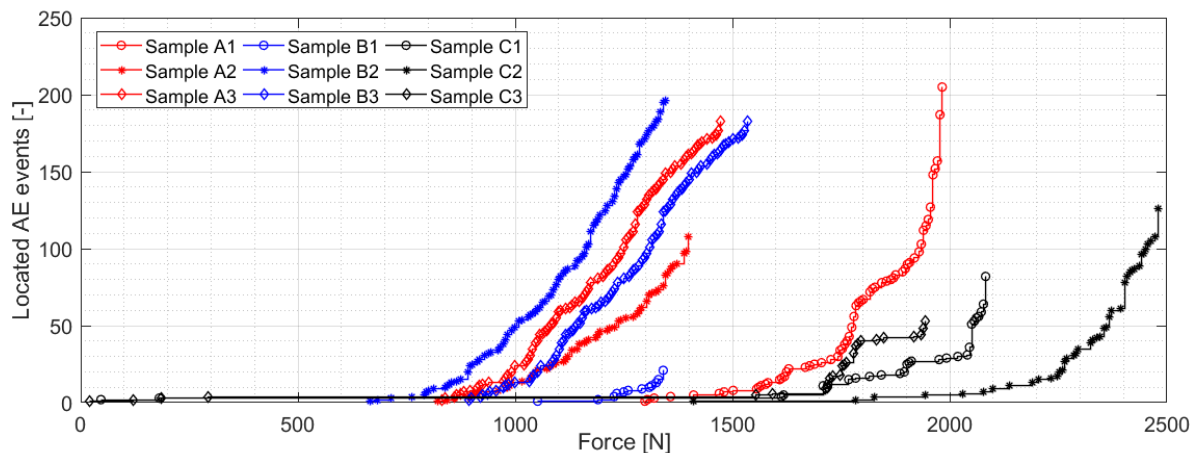


Fig. 5: Located event as the function of force for individual A/B/C production run samples

Following figure display the energy-force relation for individual samples from A/B/C series. The maximum value of released AE energy is for all samples between 10^8 and 10^9 aJ. The difference, however, lies in the character how the energy is being released during the loading process. A and B series specimen exhibit almost gradual AE energy release, with the difference in the final loading stage. While A series specimen tend to gradually continue with the cumulation of the AE events and gradual release of the AE energy, B series samples tend to suddenly lose integrity without any warning phase. A completely different behavior can be found in case of C series samples, which have considerably larger energy per event ratio with a lack of any warning phase before the integrity lose.

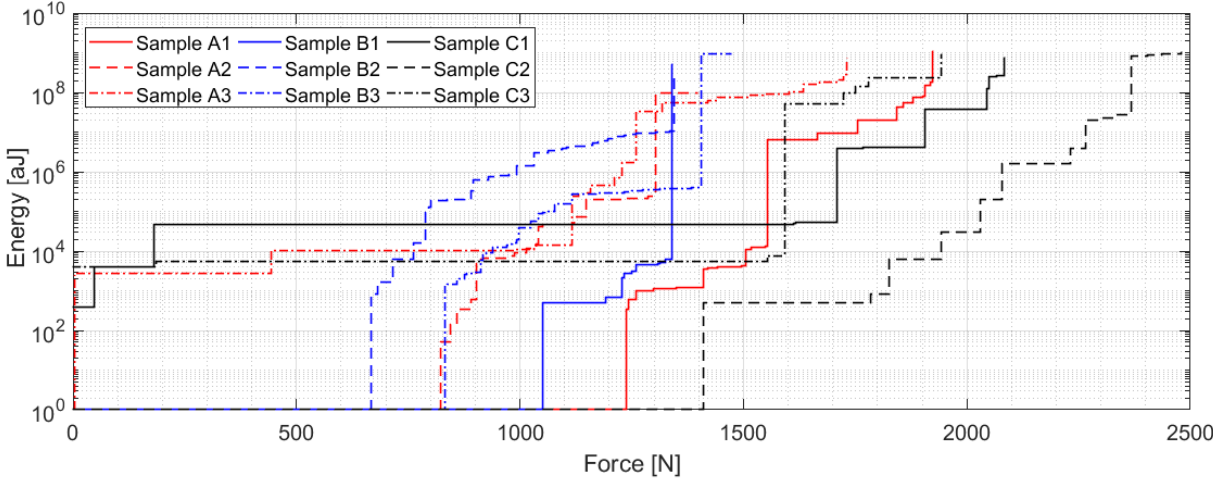


Fig. 6: Energy as the function of force for individual A/B/C production run samples

The issue of identification of failure mechanisms in composites is relatively complicated, as evidenced by a number of publications, which surprisingly do not give a clear answer in the area of amplitude and frequency spectra [11-15]. The performed unsupervised pattern recognition analysis revealed four groups of signals with characteristic properties. The signals in the first class are characterized by high amplitude in most cases exceeding $95 \text{ dB}_{\text{AE}}$ with energy value usually above $1 \cdot 10^6$ aJ and frequencies in the span from 50 kHz to 150 kHz (see Fig. 7), whereas the class also contains signals with frequency content above 300 kHz. The second class is characterized by amplitudes usually below $80 \text{ dB}_{\text{AE}}$ with AE energy in the order of thousands to tens of thousands of aJ and the frequency in the 50÷450 kHz range (see Fig. 8). The third class is represented by signals with amplitude in the $70 \div 90 \text{ dB}_{\text{AE}}$ range with AE energy in the order of ten thousand aJ and the frequency in the 50÷300 kHz range (see Fig. 9). The fourth class is characterized by signals in the $90 \div 110 \text{ dB}_{\text{AE}}$ amplitude range, AE energy in $1 \cdot 10^5 \div 1 \cdot 10^6$ aJ and with frequency in the 50÷200 kHz range (see Fig. 10).

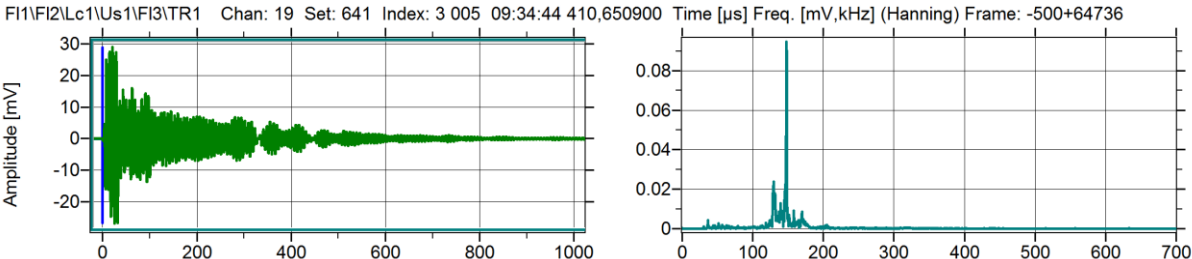


Fig. 7: Class 1 signal example

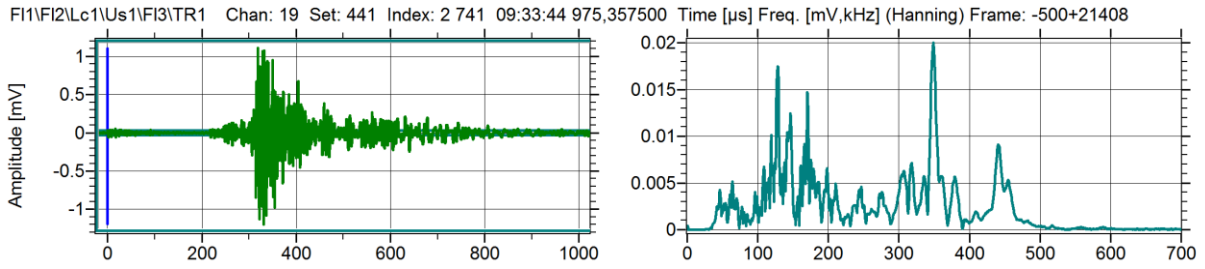


Fig. 8: Class 2 signal example

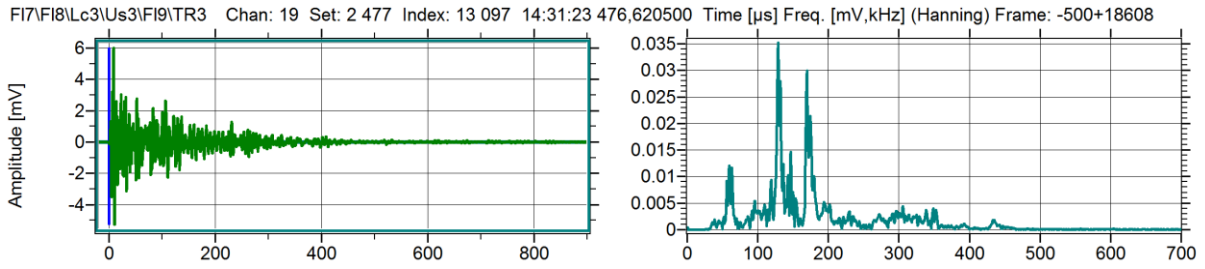


Fig. 9: Class 3 signal example

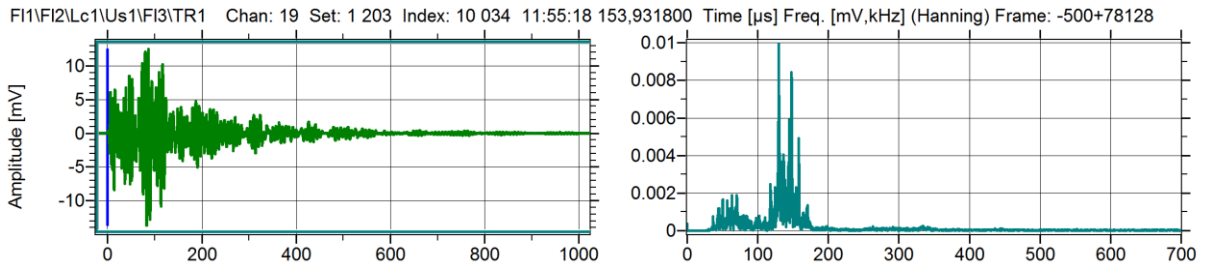


Fig. 10: Class 4 signal example

Figures 11-13 show the cluster classification of localized AE events as the function of time and distance corrected amplitude for individual A/B/C production run samples. Almost in all cases starts the damage with located events assigned to cluster 2, i.e. characterized by lower amplitudes and 50÷150 kHz frequency range, which can be most likely assigned to the matrix cracking, followed by signals with high frequency content, usually above 300 kHz, coming from fiber breakage. A similar categorization can be found in case of AE signals belonging to class 3, whose are characterized by higher amplitudes and AE energies, but slightly lower frequency ranges.

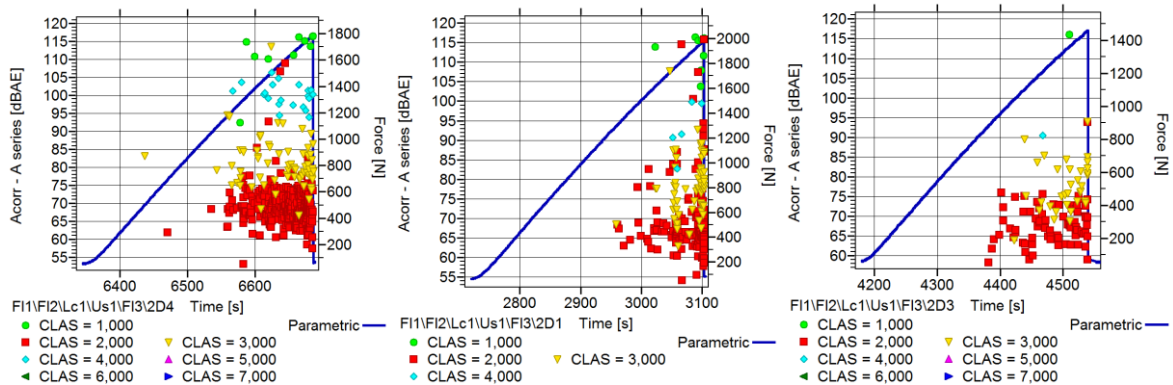


Fig. 11: A series sample results

Classes 1 and 4 on the other hand share the highest energy as well as amplitude values, while having a lower frequency range, however even in this case can be found a small group of signals with a frequency content reaching up to 450 kHz. The reason for occurrence of both low and high frequency signals in the mentioned classes lies in the overlapping of individual clusters between each other (see Fig. 3). Based on the given parameters and, at the same time, using available literature can we conclude, that classes 1 and 4 most likely represent the interface decohesion and in some cases also the fiber breakage (signals with higher frequency content). Figure 14 additionally shows the typical frequency spectrum for fiber breakage in case of C1 sample. Generally speaking, figures 11-13 show different character of the damage evolution process particularly in the percentage of the presence of class 1 and class 4 signals, which should represent the interface decohesion and higher volume fiber breakage events due to different number of unidirectional woven fabric layers with different density at the same time. Especially in case of C series samples can be the fiber breakage clearly identified by high frequency class 1 signals over 110 dB_{AE}, which start to occur near the ultimate limit of the loading force.

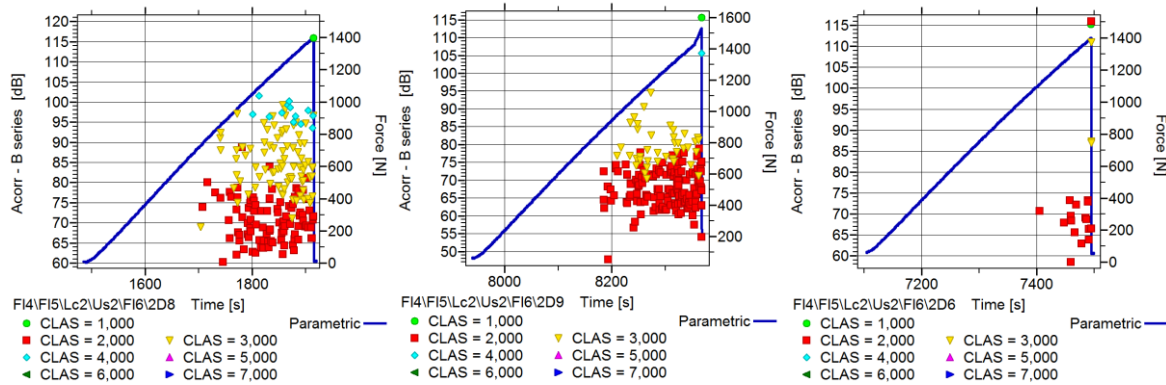


Fig. 12: B series sample results

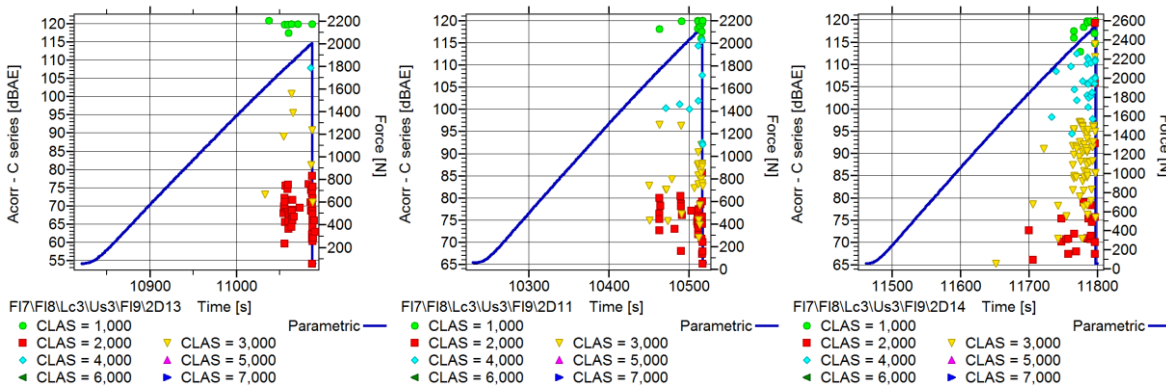


Fig. 13: C series sample results

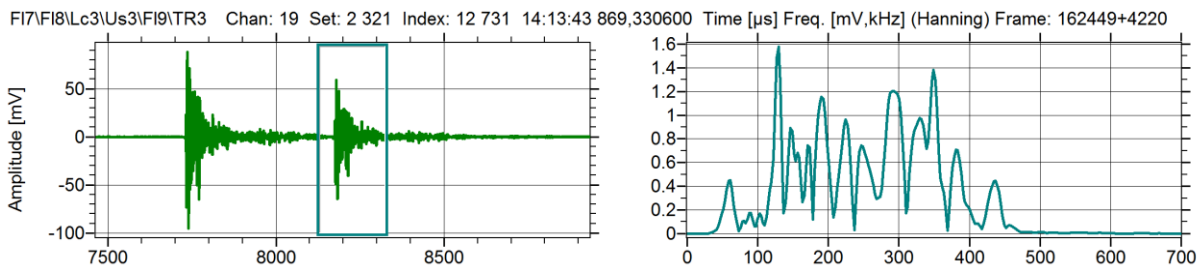


Fig. 14: Fiber breakage at 0,98*F_{max} force value with amplitude exceeding 120 dB_{AE}, Class 1 (C1 sample)

On the other hand, A series samples, especially sample A1, report a relatively large number of high frequency class 2 signals, which also belong to fiber breakage. However, as mentioned above, such signals will begin to occur after their low frequency counterparts, whose report the matrix cracking process. In conclusion we can say that the fiber breakage failure mechanism occurs in a wide spectrum of amplitudes, while the matrix cracking process occupies amplitudes up to 60÷70 dB_{AE}. AE events with higher amplitude and AE energy mainly belong to interface decohesion and/or higher volume of fiber breakages.

Conclusion

AE monitoring technique together with an unsupervised pattern recognition technique has been used to analyze the damage evolution of the three types of CFRP composite samples in order to identify the different damage mechanisms of considered materials during three point bending test. The analysis resulted in cluster classification, which to a certain extent represented matrix cracking, fiber breakage or interface decohesion. Due to a partial overlap of individual clusters between each other can be the mentioned phenomena registered in multiple clusters, which is particularly evident in the case of fiber breakage or matrix cracking. In spite of the work done, there are a number of questions, which have to be answered in a future research activities, such as more specific properties of the AE signal belonging to the fiber breakage or interface decohesion.

Acknowledgment

This work was supported by Specific Research (SP2020/23) and by project Innovative and additive manufacturing technology—new technological solutions for 3D printing of metals and composite materials - CZ.02.1.01/0.0/0.0/17_049/0008407. The authors would also like to thank the Havel Composites Ltd. company for providing the test samples and consulting during the elaboration of the paper.

References

- [1] R. Unnthorsson, T. P. Runarsson, M.T. Jonsson, Acoustic emission based fatigue failure criterion for CFRP, *Int. J. of Fat.* 30 (2008) 11-20.
- [2] J. Majko, M. Handrik, M. Vaško, M. Sága, Influence of Fiber Deposition and Orientation on Stress Distribution in Specimens Produced Using 3D Printing, *Strojnícky časopis - Journal of Mechanical Engineering*, 69 (2019), 81-88.
- [3] F. Dorčiak, M. Vaško, M. Handrik, F. Bárník, J. Majko, Tensile test for specimen with different size and shape of inner structures created by 3D printing, *Transportation Research Procedia* 40 (2019), 671-677.
- [4] J. Majko, M. Sága, M. Vaško, M. Handrik, F. Bárník, F. Dorčiak, FEM analysis of long-fibre composite structures created by 3D printing, *Transportation Research Procedia* 40 (2019), 792-799.
- [5] C. U. Grosse, *Acoustic Emission Testing*, Berlin Heidelberg: Springer-Verlag, 2018.
- [6] M. Šofer, P. Kučera, E. Mazancová, L. Krejčí, Acoustic emission and fractographic analysis of seamless steel pressure cylinders with artificial flaws under hydrostatic burst testing, *J. of Non. Ev.* 38 (2019) 84-96.

- [7] R. Čech, P. Horyl, P. Maršálek, Modelling of Two-Seat Connection to the Frame of Rail Wagon in Terms of Resistance at Impact Test, *Strojnícky časopis - Journal of Mechanical Engineering*, 66 (2016), 101-106.
- [8] R. Kocich, M. Cagala, J. Crha, P. Kozelsky, Character of acoustic emission signal generated during plastic deformation, 30th European Conference on Acoustic Emission Testing & 7th International Conference on Acoustic Emission, University of Granada, 12-15 September 2012.
- [9] J. Tang, S. Soua, C. Mares, T.-H. Gan, Pattern Recognition Approach to acoustic emission data originating from fatigue of wind turbine blades, *Sensors* 17 (2017) 2507-2519.
- [10] J.H. Vallen, G. Ruske, Acoustic emission source discrimination by analyzing short-term frequency spectra.
- [11] N. Godin, S. Huguet, R. Gaertner, Integration of the Kohonen's self-organising map and k-means algorithm for the segmentation of the AE data collected during tensile tests on cross-ply composites. *NDT & E International* 38 (2005) 299–309.
- [12] J.R. Wadim, *Acoustic Emission Applications*; D. Endeveco: San Juan Capistrano, CA, USA, 1978.
- [13] K. Komai, K. Minoshima, T. Shibutani, Investigations of the fracture mechanism of carbon/epoxy composites by AE Signal Analyses. *JSME international journal* 34 (1991) 381–388.
- [14] H.-J. Jong, Transverse cracking in a cross-ply composite laminate - detection in acoustic emission and source characterization. *Journal of Composite Materials* 40 (2006) 37–69.
- [15] M. Gresil, M.N. Saleh, C. Soutis, Transverse crack detection in 3D angle interlock glass fibre composites using acoustic emission, *Materials* 9 (2016) 699-719.